DOI: 10.1002/chem.200801273

N,*N*-Dimethylaminopropylsilane: A Case Study on the Nature of Weak Intramolecular Si···N Interactions

Michael Hagemann,[a, b] Raphael J. F. Berger,[a] Stuart A. Hayes,[a] Hans-Georg Stammler,[a] and Norbert W. Mitzel*[a, b]

Dedicated to Professor Peter Jutzi on the occasion of his 70th birthday

Abstract: *N*,*N*-Dimethylaminopropylsilane $H_3Si(CH_2)_3NMe_2$ was synthesised by the reaction of $(MeO)_3Si(CH_2)_3NMe_2$ with lithium aluminium hydride. Its solid-state structure was determined by X-ray diffraction, which revealed a five-membered ring with an Si···N distance of 2.712(2) Å. Investigation of the structure by gas-phase electron diffraction (GED), ab initio and density functional calculations and IR spectroscopy revealed that the situation in the gas phase is more complicated, with at least four conformers present in appreciable quantities. Infrared spectra indicated a possible Si···N interaction in the Si–H stretching region (2000–2200 cm^{-1}), as the approach of the nitrogen atom in the five-membered ring weakens the bond to the hydrogen atom in the *trans* position. Simulated gas-phase IR spectra generated from ab initio calculations (MP2/TZVPP) exhibited good agreement with the experimental spectrum. A method is proposed by which the fraction of the conformer with a five-membered ring can be determined by a least-squares fit of the calculated to experimental absorption intensities. The abundance of this conformer was determined as 23.7(6)%, in good agreement with the GED value of 24(6)%. The equilibrium Si···N distance predicted by theory for the gas-phase structure was highly variable, ranging from 2.73 (MP2) to 3.15 Å (HF). The value obtained by GED is 2.91(4) Å, which could be confirmed by a scan of the potential-energy surface at the DF-LCCSD[T] level of theory. The nature of the weak dative bond in $H_3Si(CH_2)_3NMe_2$ can be described in terms of attractive inter-electronic correlation forces (dispersion) and is also interpreted in terms of the topology of the electron density.

Keywords: ab initio calculations · conformation analysis · electron diffraction · IR spectroscopy · silanes

Introduction

Organosilicon compounds have attracted attention for a number of decades, because they have found applications in both industry and everyday life. Examples include silicones in the form of the materials themselves and as cross-linkers; additives for paints, inks, adhesives (adhesion promoters) and cosmetics; and water-repellent agents.[1] Some of the silanes already in use are also hypervalent silicon compounds, which are gaining in importance.

In recent years so called α-silanes, that is, silanes with a donor function in geminal position relative to the silicon centre, are replacing and complementing the industrially used organofunctional silanes with donor functions in the δ position due to their higher reactivity.[1] The fact that the properties of silanes with donor functions in the β position differ strongly from those with a donor in δ position was first established in the 1950s.[2] Later Kostyanovskii et al. examined the basicity of amines with a group 4 element in geminal position and found that amines with geminal acceptor atoms showed reduced basicity. This was explained by the formation of a geminal donor–acceptor interaction between the group 4 and nitrogen atoms[3] and was contrasted in this respect to the behaviour of the γ-silanes. This interaction between silicon and nitrogen leads to pentacoordinate Si atoms, which were established to undergo much faster nucleophilic substitution reactions than tetra- or hexacoordinate derivatives.[4]

[a] Dr. M. Hagemann, Dr. R. J. F. Berger, Dr. S. A. Hayes, Dr. H.-G. Stammler, Prof. Dr. N. W. Mitzel
Fakultät für Chemie, Universität Bielefeld
Universitätsstraße 25, 33615 Bielefeld (Germany)
Fax: (+49) 521 106 6026
E-mail: mitzel@uni-bielefeld.de

[b] Dr. M. Hagemann, Prof. Dr. N. W. Mitzel
NRW Graduate School of Chemistry, Universität Münster
Corrensstraße 36, 48149 Münster (Germany)

Supporting information for this article is available on the WWW under http://dx.doi.org/10.1002/chem.200801273

 © 2008 Wiley-VCH Verlag GmbH & Co. KGaA, Weinheim WILEY InterScience DISCOVER SOMETHING GREAT

Many intramolecular datively bonded ring systems are known,[5] but no detailed studies on simple flexible systems and the relative stability of ring versus open chain conformers have been performed so far.

We recently demonstrated that such silicon–donor interactions strongly depend on the substitution patterns of the silicon and donor atoms, as well as on the nature of the spacer function bridging these atoms. This work was done experimentally and theoretically by analysing model compounds including $F_3SiCH_2NMe_2$,[6] $(F_3C)F_2SiONMe_2$,[7] $F_3SiN(R)NMe_2$ (R = Me, $SiMe_3$, $SnMe_3$),[8] $MeHSi[ON(BH_3)Me_2]_2$[9] and $ClH_2SiONMe_2$.[10] It transpires that the composition of the spacer function is highly important for enabling or disabling a silicon–donor interaction. No example of an attractive silicon–donor interaction in geminally donor substituted silanes with a methylene unit (CH_2) as spacer function is known. In contrast, the hydroxylamine $(F_3C)F_2SiONMe_2$ with an O spacer exhibits a short Si···N distance and an extremely acute angle at the spacer function (solid state: 1.904(2) Å, 74.1(1)°).[7] However, as for other compounds exhibiting dative bonding,[5] this effect is exaggerated in the solid state and the Si-O-N angle of the above compound in the gas phase was determined to be 84(3)° for the *anti* conformer and 88(2)° for the *gauche* conformer.[7]

Abstract in Midwestern Bavarian: *Mia hamma des* N,N-*Dimethylaminobrobilsilan ausm* $(MeO)_3Si(CH_2)_3NMe_2$ *und am Liziumaluminiumhidrid gmachd. Wenn ma des im fesdn Zuaschdand ois oanzeine Grisdalle durchleichd (OGD), kimds auf, das do Ringal vo jäweis fimbf Adome drinna hand, bei dene wo de Siliziumadome und de Schdigschdoffadome grod 2.712(2) Å ausananda hand. Ois a Gas, eleggdrona-gschdraad (GES), IR schbeggdrosgobbisch undasuachd un ab-initio un Dichtefunktional-massig berächned, kimmd gee aussa, das do guadding drei andaschde Konformera, ois wia des oane mid de Ringal a no drinna hand. Am IR kend mas deswengn scho, das do de Ringal drinn hand, wei de symmädrischen und de ned-symmädrischen Si–H Schdreggschwingunga um 200 Weinzoin ausanandagengand. Vo dem hea muas des a so sei, das do no a Schdiggschdoff an des Silizium hikoordiniad. Do is hoid naa des Wassaschdoffadom auf da drendan Seidn vom Schdiggschdoffadom nimma so fest hibundn an des Siliziumadom herend. Wenn mia ofd no de IR schbeggdren ausdarächned (MP2/TZVPP) bassds guad mid den zam wo ma gmessn ham, awa das des naa a aggradd bassd, muas ma no zeaschd ausm IR Schbeggdrum aussadalesn wiavui vohaidnissmassig vo dem Konformer mid de Ringal drinna is. Des sei Vohaidniss hamma nochm gleansdn Fääla im Kwadrad oobassd. Ganz zlezd is aussakemma, das ma am IR 23.7(6) % Ringal sichd und bei da GES 24(6) %. Beim Berächna, wia weid das des Schdigschdoffadom vo dem Siliziumadom in dene Ringal wegga is, is vo 2.73 bis 3.15 Å (HF, MP2) ausanandaganga. Bei da GES hand do 2.91(7) Å aussakemma.*

The loss of the silicon–nitrogen interaction when the oxygen spacer is replaced by a methylene group could be due to any one of a number of reasons. These include the greater rigidity of the methylene spacer, rearrangement of charge, which would alter the electrostatic forces, and reduced electron deficiency of silicon making it less inclined to accept electron density from nitrogen by way of a dative bond. By increasing the number of spacer units, it should be possible to evaluate the importance of the rigidity of the CH_2 spacer. This paper therefore presents a detailed investigation of the structure and conformational preference of $H_3Si(CH_2)_3NMe_2$ (**3**), in which the presence of three CH_2 spacer groups allows greater freedom for the Si···N interaction. Where relevant, the results are also compared with related compounds $H_3SiCH_2NMe_2$ (**1**), which was described earlier,[12] and $H_3Si(CH_2)_2NMe_2$(**2**), which we prepared for spectroscopic comparison. Note that, in contrast to earlier studies on compounds with rigid backbones between the Si and N atoms, such as 1,8-naphthyl groups,[5a] the highly flexible backbone of **3** does not enforce an Si···N interaction, as the molecules can adopt linear (open chain) conformations and ring-type conformations in which an intramolecular interaction may take place.

Results and Discussion

Synthesis: The syntheses of the model compounds $H_3Si(CH_2)_nNMe_2$ with $n=1$ (**1**), 2 (**2**) and 3 (**3**) are straightforward procedures. The corresponding methoxy-substituted silanes $(MeO)_3Si(CH_2)_nNMe_2$ ($n=1$–3) can be reduced with lithium aluminium hydride ($LiAlH_4$) to give the corresponding hydrido silanes (Scheme 1).

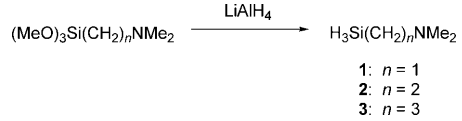

Scheme 1. Synthesis of $H_3Si(CH_2)_nNMe_2$, with $n=1$ (**1**), 2 (**2**) and 3 (**3**).

Compound **1** was analysed and described earlier,[12] but we list some of its properties here for the sake of discussion. Compounds **2** and **3** are liquids at ambient temperature with boiling points of 47 °C at 530 mbar for **2** and 60 °C at 200 mbar for **3**. The compounds were purified by fractional condensation on a high-vacuum line prior to analysis.

NMR spectroscopy: NMR spectroscopic parameters such as chemical shifts and coupling constants are very sensitive to changes in the electronic environment of the observed nucleus. Thus, a change in NMR properties may provide information about the conformation of the molecule and a possible Si···N interaction. Table 1 lists some experimental multinuclear NMR spectroscopic data of **1**–**3**.

Neither the chemical shifts nor the $^1J_{SiH}$ coupling constants change in such a way upon increasing the chain

 © 2008 Wiley-VCH Verlag GmbH & Co. KGaA, Weinheim

Table 1. Selected NMR spectroscopic data of **1**–**3**.

$H_3Si(CH_2)_nNMe_2$	Solvent	$\delta(^{29}Si)$ [ppm]	$\delta(^1H,SiH_3)$ [ppm]	$^1J_{SiH}$ [Hz]
1: $n=1$[12]	C_6D_6	−66	3.63	196
2: $n=2$	$CDCl_3$	−62	3.37	195
3: $n=3$	$CDCl_3$	−60	3.44	193
3: $n=3$	[D_8]toluene	−62	3.77	193

length that a conclusion on the coordination number of silicon can be drawn. To gain some insight it is helpful to compare these results to those of similar compounds which lack donor functions. The ^{29}Si chemical shifts of H_3SiCH_3 and $H_3SiCH_2CH_2CH_3$ are −65.2 and −59.4 ppm, respectively,[13] and the similarity of these values to those in Table 1 suggest that no significant interactions are present. However, two important intramolecular effects might have a strong influence on the ^{29}Si chemical shifts. On the one hand there is an inductive effect, which leads to deshielding of the Si nucleus by bond polarisation and therefore to a low-field shift of the ^{29}Si signals. In **1** this effect should be relatively strong, whilst in **3** it should be weaker. On the other hand, a silicon–nitrogen interaction leads to a pentacoordinate silicon centre and consequently to a high-field shift of the ^{29}Si signal. These effects may cancel each other out, so that information on the existence of a Si···N interaction cannot be concluded from these NMR data.

Another piece of evidence that, if any, only a very weak Si···N interaction may be present, is the observation that upon cooling **3** to 220 K, the NMR spectra do not exhibit large changes (Figures 1 and 2). In general, the NMR spectroscopic data of pure **3** differ little from those in solution. In the ^{29}Si NMR spectrum small shifts of 2 ppm ([D_8]toluene) and 3 ppm (neat sample) of the signals towards higher field is observed after cooling the sample. Ab initio calculations and gas-phase electron diffraction (GED) analysis indicate that many conformers are present in the gas phase, and that cyclic conformer **3a** may have the lowest zero-point energy. This change in the ^{29}Si chemical shift may, therefore, be due to increased abundance of the cyclic conformer.

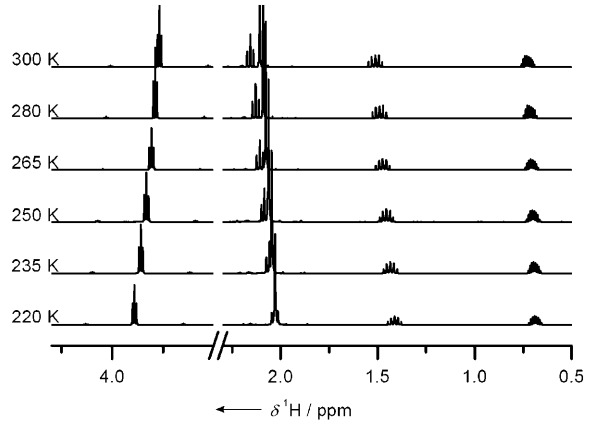

Figure 1. Variable-temperature ^1H NMR spectra of **3** (in [D_8]toluene).

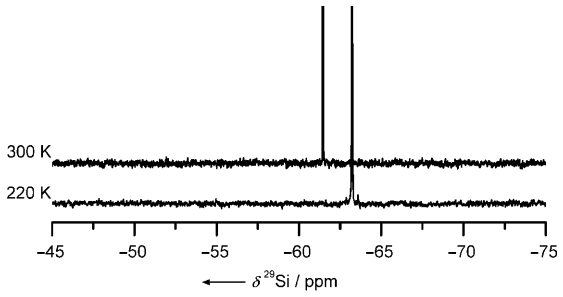

Figure 2. ^{29}Si NMR spectra of **3** at 220 and 300 K (in [D_8]toluene).

In summary, the multinuclear NMR spectroscopic data are inconclusive but indicate that, in solution, **3** is in a state of dynamic equilibrium between cyclic and open-chain conformers. This dynamic process, even at low temperatures, appears to be too fast for observation of the single species by NMR methods.

Crystal structure: A single crystal was grown in situ on the diffractometer from a solid/liquid equilibrium established at a temperature of −102 °C. Compound **3** crystallises in the tetragonal space group *I*4*m*, with eight molecules in the unit cell. The structure of **3** is depicted in Figure 3, and selected structural parameters are listed in Table 2. Compound **3** crystallises as a monomeric, five-membered-ring conformer, with no intermolecular distances shorter than the sum of the

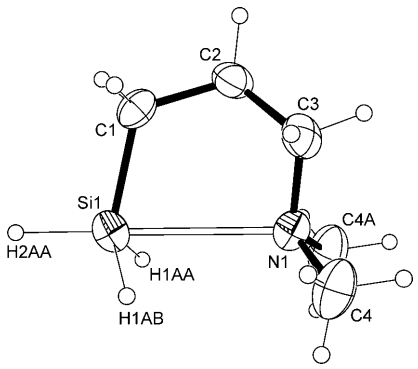

Figure 3. X-ray structure of $H_3SiCH_2CH_2CH_2NMe_2$ (**3**) with thermal ellipsoids at 50% probability.

Table 2. Selected bond lengths [Å] and angles [°] of $H_3SiCH_2CH_2CH_2NMe_2$ (**3**) in the solid state as determined by X-ray diffraction.

Si1···N1	2.719(2)	H2AA-Si1-N1	179.6(13)
Si1−H2AA	1.47(3)	H2AA-Si1-C1	103.5(13)
Si-H1AB/H1AA	1.37(2)	Si1-C1-C2	118.6(2)
Si1−C1	1.875(5)	C1-C2-C3	112.4(4)
C1−C2	1.507(5)	C2-C3-N1	108.1(3)
C2−C3	1.518(5)		
C3−N1	1.476(4)		
N1−C4/C5	1.451(2)		

 © 2008 Wiley-VCH Verlag GmbH & Co. KGaA, Weinheim

van der Waals radii of the respective atoms. The intramolecular Si···N distance of 2.712(2) Å is shorter than in the gas-phase structure of $H_3SiCH_2NMe_2$ (2.828(7) Å).[12] The H2AA-Si1-N1 angle is very close to 180° (179.6(13)°). These are important structural features consistent with an attractive Si···N interaction. Since the molecule lies on a crystallographic mirror plane, atoms C1 to C3 are disordered, and the angles to hydrogen atoms H1AA and H1AB are uncertain. However, the coordination geometry about the silicon atom is between tetrahedral and trigonal bipyramidal, with the silicon atom positioned 0.349(13) Å above the plane defined by H1AA, H1AB and C1.

IR spectroscopy: The solid-state, liquid and gas-phase IR spectra of **3** each show two strong absorption bands in the region between 1950 and 2250 cm^{-1} (Figure 4), which can be

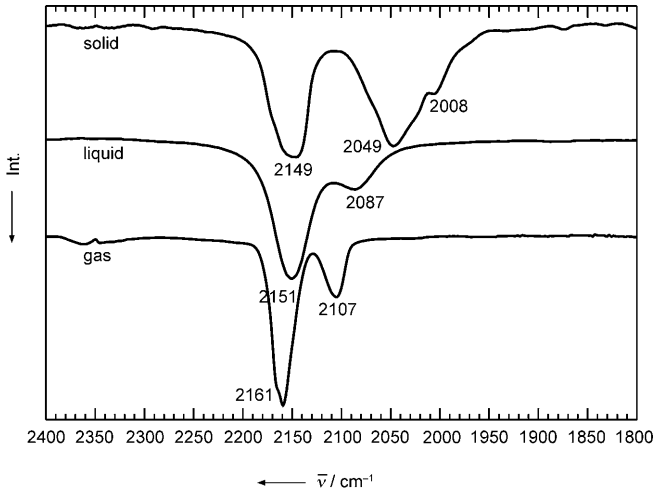

Figure 4. Detail of the solid-state, liquid and gas-phase IR spectra of **3**, showing the Si–H stretching region. The numbers refer to the maxima of the neighbouring peaks.

attributed to Si–H stretching modes of the silane group. Spectra were calculated for five-membered ring structure **3a**, and one peak was assigned to the Si–H stretch involving the hydrogen atom pointing away from the nitrogen atom (ν_{trans}(SiH), 2008–2107 cm^{-1}). The other band was assigned to overlapping contributions of the symmetric and asymmetric stretching modes of the remaining SiH_2 moiety ($\nu_s(SiH_2)$ and $\nu_{as}(SiH_2)$, 2149–2161 cm^{-1}). Comparison of the experimental and simulated spectra reveals a considerable mismatch of the relative intensities of the two observable peaks, as shown in Figure 5, which is more pronounced in the gas-phase and liquid-phase spectra than in the solid-state spectrum. To explain this observation, a systematic conformational analysis of 216 possible open-chain conformers was performed. This resulted in finding eight different low-energy conformers including **3a** (the five-membered-ring conformer) and seven open-chain conformers **3b**–**h** that are distinct minima on the potential-energy surface (see Figure 6).

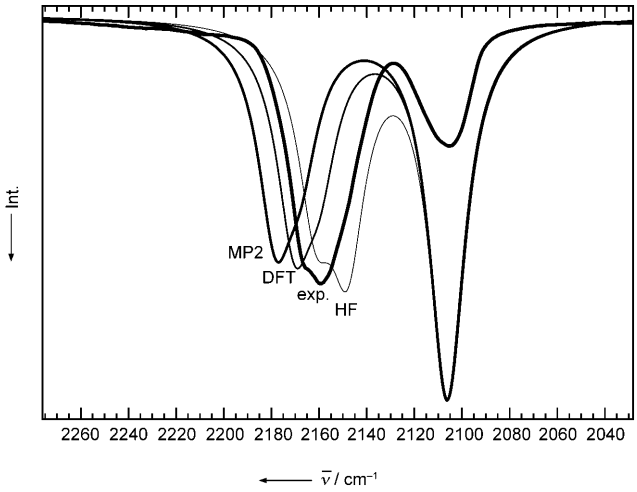

Figure 5. Gas-phase IR spectrum of **3** and simulated (see text) IR spectra for **3a** showing the Si–H stretching region. The calculated frequencies were scaled (HF 0.933, MP2 0.948, DFT 0.972) to match the experimentally observed peak at 2107 cm^{-1}. Lorentzian functions with a fixed half-width were used for simulation of peak shapes. Note the mismatch in relative intensities of the calculated bands with respect to the experimentally observed bands, and the variation in wavenumber differences with respect to the employed method.

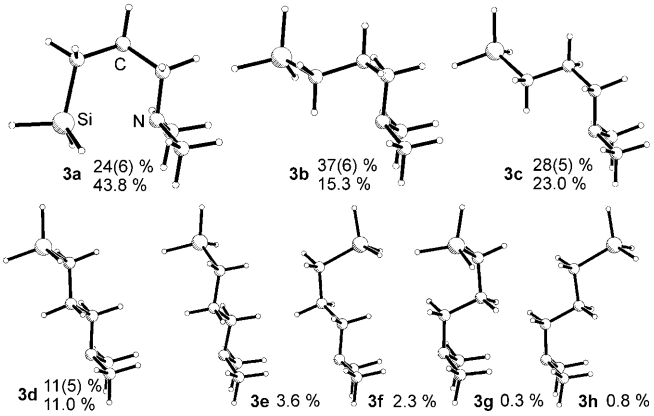

Figure 6. Conformers of **3** showing the molar fraction of each as determined by GED (upper value, where the number in parentheses is 2σ) and calculated at the MP2/TZVPP level of theory.

Spectral fitting: The relative abundance of conformer **3a** at ambient temperature was determined from gas-phase IR spectra by employing a least-squares fitting procedure. For that purpose, IR spectra were simulated for open-chain conformers **3b**–**h** by using the calculated intensities for the peak heights and a constant value for the peak widths. These simulated spectra were then combined by using a Boltzmann weighting with the Boltzmann factors based on calculated $\Delta G_0^{298.15}$ values (MP2/TZVPP). The transmittance ($\tau = I/I_0$) values from seven separate IR spectra were transformed into absorbance values ($A = -\lg\tau$), prior to the fitting procedure. The ratio of conformer **3a** to those of the open-chain conformers was then determined by a least-squares fit of the two simulated IR spectra to each of the gas phase IR spectra in the region from 2050 to 2250 cm^{-1}. The gas-phase

 © 2008 Wiley-VCH Verlag GmbH & Co. KGaA, Weinheim

abundance of **3a** at ambient temperature determined in this way is 23.7(6)%, whereby the variation from one spectrum to another is less than one standard deviation. Figure 7 shows the individual simulated spectra, the resulting fitted

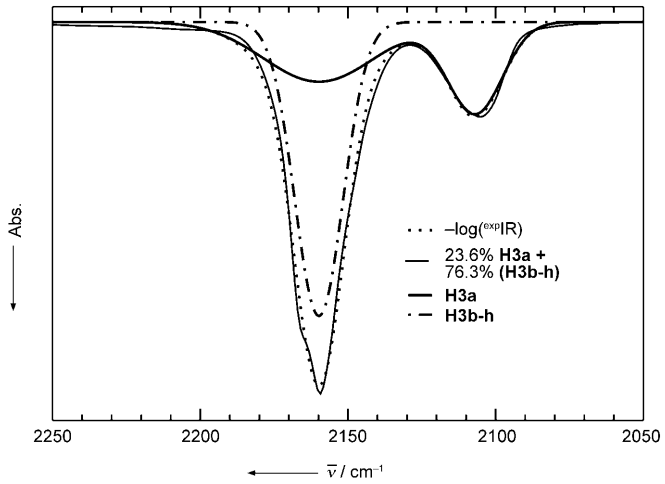

Figure 7. Gas-phase IR spectrum of **3** and functions used in the fitting procedure for determination of the relative fraction of **3a** (the five-membered-ring conformer) in **3**. The IR intensity data and the scaled relative wavenumbers in the region of 2200 to 2140 are taken from ab initio calculations (MP2).

simulated spectrum and the experimental spectrum. Figure 8 compares the gas-phase IR spectrum with the simulated IR spectra over a broader range of frequencies (500–3100 cm^{-1}), also obtained by using the fitted ratio of **3a**. Interestingly, Gaussian functions gave a closer fit of the peak shapes to the experimental spectra than Lorentzian functions (see Supporting Information for a detailed description of the fitting procedure).

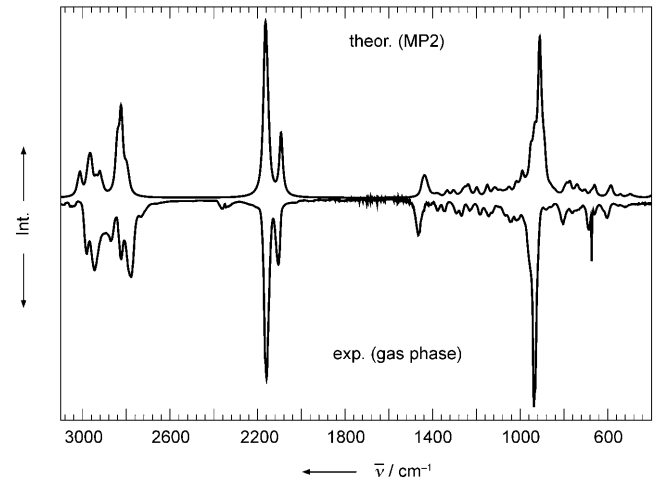

Figure 8. Gas-phase IR spectrum of **3** versus a linear combination of simulated IR spectra of conformers **3a**–**h**, also obtained by using the fitted ratio of conformer **3a**. The asterisk denotes a band originating from CO_2.

Phase dependence of IR spectra: The spectra show different relative intensities of the two Si–H stretching bands that reflect different abundances of conformers in the various phases and at various temperatures. From the crystal structure determination, only cyclic conformer **3a** is present in the crystal. The wavenumber difference $\Delta\tilde{\nu}$(SiH) between the ν_{trans}(SiH) vibrational mode and the $\nu_{as}(SiH_2)$ and $\nu_s(SiH_2)$ vibrational modes is 54 cm^{-1} in the gas phase, 64 cm^{-1} in the liquid phase and 100 cm^{-1} in the solid state (see Figure 4). This variance indicates the flexibility (weakness) of the Si···N interaction in this compound. In summary, the Si···N interaction appears to be considerably affected by the state of aggregation, although effects of thermal motion may also play a role.

Dependence of calculated IR spectra on level of theory: The calculated values of $\Delta\tilde{\nu}$(SiH) also vary with the employed level of theory. As shown in Figure 5, $\Delta\tilde{\nu}$(SiH) increases with an increasing contribution of dynamical correlation inherent in the level of theory (as in the sequence HF, DFT, MP2). Parallel to the increase in $\Delta\tilde{\nu}$(SiH) the calculated Si···N distance decreases (Figure 9). Because Hartree–Fock calculations do not account for dispersion forces, it may be concluded that far-reaching, weak interactions like van der Waals forces are crucial for the occurrence of Si···N interactions in **3**.

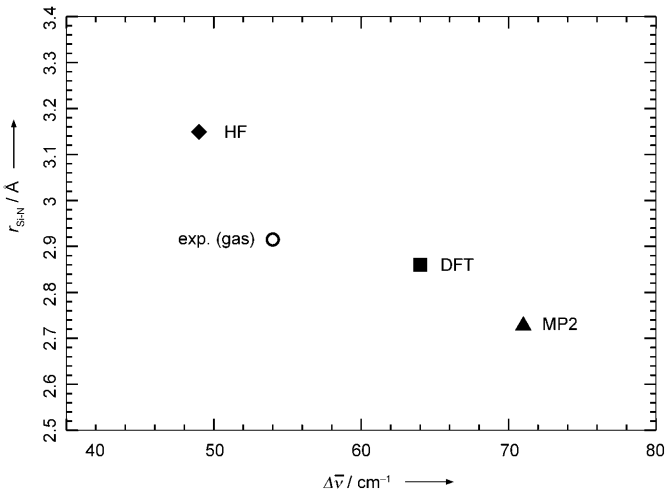

Figure 9. Wavenumber difference between the ν_{trans}(SiH) vibrational mode and the $\nu_{as}(SiH_2)$, $\nu_s(SiH_2)$ modes plotted against the equilibrium distance between silicon an nitrogen in **3a**, calculated at different levels of theory. For comparison, the experimental r_{h1} value from this work is also depicted. Both the Si···N distance and the value of $\Delta\tilde{\nu}$(SiH) can be viewed as indicators for the strength of the Si···N interaction. (For a detailed description of the levels of theory employed, see Computational Details.)

Theoretical structures and relative energies: To investigate the gas-phase composition of **3** in terms of conformations and respective molecular structures, the IR and GED investigations were complemented with first-principles calculations. The following questions were addressed:

 © 2008 Wiley-VCH Verlag GmbH & Co. KGaA, Weinheim

1) Which conformers are of major importance for the gas-phase composition?
2) What is their respective ratio in the equilibrium under the experimental conditions?
3) Which kind of structural restraints can be used for the GED analysis and how do the predicted geometries compare to those from the GED refinement?
4) Is there an intramolecular Si···N interaction, and if so which type of interaction is it?

Theoretical conformational analysis: Both NMR and IR spectroscopy confirm that more than one conformer is of importance for a proper description of **3a** in the gas phase and in solution. To account for all important conformers, all 216 possible molecular geometries arising from all combinations of the three dihedral angles θ_i ($i=1$, 2, 3; see Scheme 2) with $\theta_i \in \{0, 60, 120, 180, 240, 300\}$ were generated automatically. In a first step all chiral pairs were identified and all structures containing atom pairs lying closer than 0.5 Å to each other were rejected. This resulted in 80 molecular geometries including four C_s-symmetric conformers and 76 with a chiral counterpart. To restrict this number further, conformations with non-eclipsed configurations were chosen; this yielded eight chiral pairs and one C_s-symmetric conformer. However, out of interest, the three C_s-symmetric conformers which were rejected in the previous step were also chosen for further investigation. These 12 (neglecting chirality) different conformers were first optimised with respect to their geometries by using an efficient DFT method [RI-DFT(BP86)/SV(P)], and second by using an accurate MP2 method (RI-MP2(fc)/TZVPP). At the MP2 level of theory the three C_s-symmetric confers (those having an eclipsed conformation) and one asymmetric conformer did not correspond to minima on the potential-energy hypersurface, so seven asymmetric (**3a**–**g**) and one C_s-symmetric (**3h**) conformers remained for further investigation (Figure 6).

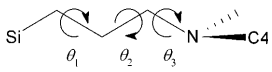

Scheme 2. Definition of dihedral angles θ_i used for the description of the conformers of $H_3SiCH_2CH_2CH_2NMe_2$. θ_3 is the C-C-N-C(4) dihedral angle.

Theoretical estimation of conformer ratios: Total energy differences from geometry optimisations yield ΔE, and rotational and vibrational contributions from the vibrational frequency analysis $\Delta G_0^{298.15}$, values. Using these calculated energies and applying a Boltzmann distribution to the abundances of the conformers allows the respective ratios in thermodynamic equilibrium to be estimated (Table 3).

Calculated structure of conformer 3a: The calculated equilibrium structure of **3a** showed the largest variations of all conformers under consideration between the different levels of theory. Table 4 lists some selected structural parameters for this conformer (numbering scheme according to the crystal structure in Figure 5). The largest deviations are found in the parameters that are influenced strongly by an intramolecular Si···N interaction. The shortest Si···N distance is predicted by the MP2 calculation; this again reflects the importance of dispersion interactions, which are known to be overestimated by MP2.[14]

Si···N potential-energy curve of 3a: The ab initio Si···N deformation potential of **3a** (Figure 10) is very shallow. Any

Table 4. Selected structural parameters of five-membered-ring conformer **3a** (bond lengths [Å] and angles [°]). The atoms are numbered according to Figure 3.

	HF	DFT	MP2
Si···N	3.149	2.858	2.728
Si–C1	1.895	1.894	1.898
Si–H1	1.488	1.502	1.494
C3–N	1.452	1.452	1.459
C4–N	1.445	1.444	1.453
C4A–N	1.446	1.445	1.454
C1–C2	1.534	1.525	1.528
C2–C3	1.524	1.518	1.520
H1-Si-C1	106.8	105.3	104.2
H1-Si-N	175.6	177.9	178.4
C1-C2-C3	114.4	112.6	110.9
C2-C3-N	113.3	111.6	110.2
C1-C2-C3-N	67.1	61.8	60.7
Si-C1-C2-C3	−61.4	−54.6	−52.9
C4-N-C3-C2	78.9	78.7	79.6

Table 3. Equilibrium energy differences ΔE [kJ mol^{-1}], calculated at various levels of theory for each conformer of **3**, and free energy differences $\Delta G_0^{298.15}$ [kJ mol^{-1}], calculated at the MP2 level of theory by invoking the rigid-rotor and harmonic-oscillator approximations. Uncertainties in the GED values correspond to 2σ.

	HF ΔE	DFT ΔE	MP2 ΔE	HF $\Delta G_0^{298.15}$	DFT $\Delta G_0^{298.15}$	MP2 $\Delta G_0^{298.15}$	HF ratio	DFT ratio	MP2 ratio	GED ratio	IR ratio
3a	(0.0)	(0.0)	(0.0)	(0.0)	(0.0)	(0.0)	11.9	16.3	43.8	24(6)	23.7(6)
3b	−0.9	4.4	7.6	−3.1	0.6	3.9	18.5	14.4	15.3	37(6)	–
3c	0.9	1.8	8.0	−0.4	-2.4	2.6	12.8	23.6	23.0	28(5)	–
3d	−3.4	2.8	11.0	−6.2	−7.3	4.8	22.0	30.1	11.0	11(5)	–
3e	2.5	7.0	14.8	−0.5	4.1	7.8	13.2	5.2	3.6	–	–
3f	1.9	6.4	13.6	1.1	3.6	9.0	9.2	6.1	2.3	–	–
3g	6.9	11.9	20.1	3.9	9.1	13.8	4.1	0.8	0.3	–	–
3h[a]	0.8	7.2	16.1	−2.1	4.1	9.9	8.4	2.6	0.8	–	–

[a] C_s-symmetric.

© 2008 Wiley-VCH Verlag GmbH & Co. KGaA, Weinheim

weak forces can therefore influence the molecular structure considerably, and the differences between the HF and MP2 geometries can be interpreted as an effect emerging from the neglect and overestimation of dispersion-type interactions in HF and MP2 theory,[14] respectively (as discussed above for the IR spectra). This view is confirmed by the results of coupled-clusters calculations (CCSD[T], MOLPRO[15]). Expectedly, the overestimation of correlation contributions (and hereby of the attractive part of the inter-electronic correlation, i.e., the dispersion contribution) by the MP2 calculation is (over)compensated by inclusion of triple excitations in the cluster expansion, which leads to a minimum-energy Si···N distance of about 2.9 Å, which lies between the corresponding HF and MP2 values. However, the small 2-norm of the t_1 vector of the coupled-cluster calculation (0.005) clearly shows that the large deviation between HF and MP2 equilibrium geometries is not a consequence of an inappropriate single-reference ansatz, but rather a rapid convergence of geometry and potential energies within the series HF, MP2, CCSD[T] can be expected. Already, the relative stability of **3a** at the HF level of theory (see Table 3) demonstrates that electrostatic interactions are important. Due to the large Si···N distance of 2.73–3.14 Å any significant p→σ* interaction between the nitrogen lone pair and the antibonding Si–H orbital is unlikely. In summary, the Si···N interaction in **3a** can be regarded as a synergism of conformational flexibility with electrostatic and dispersion (van der Waals) interactions.

Gas-phase electron diffraction (GED): Electron diffraction data were acquired for **3** and interpreted in terms of four conformers, **3a–d** (Figure 6), which were each calculated at the MP2/TZVPP level to have greater than 5% abundance at 298 K. The geometries of all four conformers were described in terms of 55 independent parameters, all of which were refined by the SARACEN method,[16] with incorporation of flexible restraints derived from fully optimised geometries at the MP2/TZVPP level of theory.

The final experimental and difference molecular-intensity curves are shown in Figure 11, whilst those for the radial-distribution function are shown in Figure 12. The conformer ratios were determined by an iterative process, whereby the *R* factor was determined as a function of the ratio of a given conformer, with this ratio fixed to the minimum in the corresponding curve, repeating for each degree of freedom until self-consistent. This yielded the set of curves shown in Figure 13.

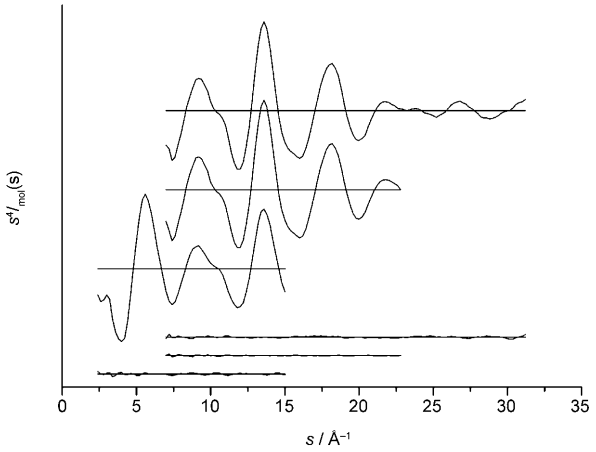

Figure 11. Experimental and difference (experimental minus theoretical) molecular-intensity curves for **3**.

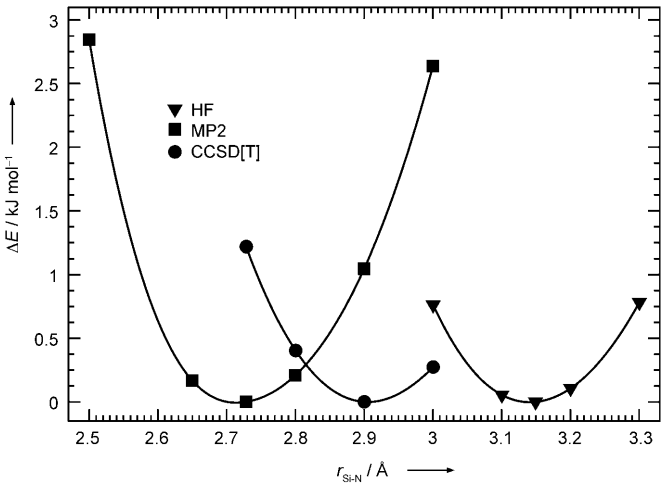

Figure 10. Relative ab initio potential-energy curve for the Si···N distance in **3a**. The experimentally determined equilibrium distance of 2.91(4) Å lies approximately between the HF and MP2 values. The large uncertainty in the GED value can be explained by the shallowness of the curve, which reflects the conformational flexibility of **3**. Due to this shallowness the Si···N distance is particularly sensitive to small energetic effects such as inter-electronic correlation.

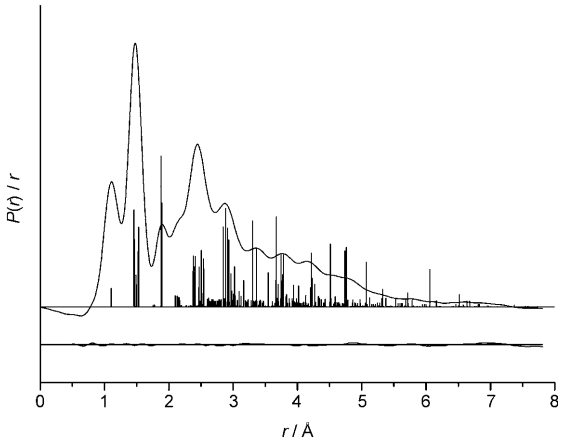

Figure 12. Experimental and difference (experimental minus theoretical) weighted radial-distribution function for **3**. Molecular scattering intensities were multiplied by $s\cdot\exp[(-0.00003s^2)/(Z_{Si}-f_{Si})(Z_C-f_C)]$ prior to Fourier inversion.

The molar fraction of **3a** was determined to be significantly lower than that predicted theoretically (24(6) vs 44%), but is in good agreement with the value of 23.7(6)% estimated by fitting IR intensities for the Si–H stretches.

 © 2008 Wiley-VCH Verlag GmbH & Co. KGaA, Weinheim

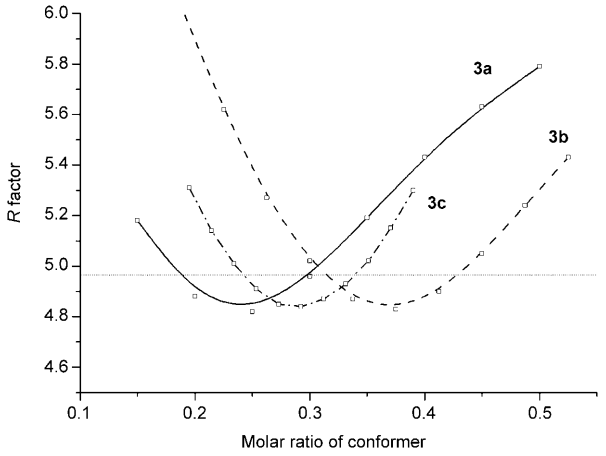

Figure 13. R_G factor as a function of the molar fraction of **3a** (solid), **3b** (dashed) and **3c** (dot-dashed). The dotted line is the 95% confidence limit (2σ), given by an R-factor ratio of 1.03, as determined from Hamilton's tables.[15]

The molar ratio of **3b** was correspondingly much greater than predicted (37(6) vs 15%), whilst the molar fractions of two remaining conformers did not differ significantly. The GED values of selected internuclear distances in **3a** and **3b** are shown alongside the corresponding theoretical values in Figure 14. In general, the GED structure parameters are close to those obtained at the MP2/TZVPP level of theory, the only significant difference being the Si···N distance of 2.91(4) Å, which compares to 2.73 Å by MP2 theory, a value which was clearly confirmed by CCSD[T] calculations (see section Si···N Potential-Energy Curve of **3a**). During the refinement it was observed that the Si···N distance is correlated to the fraction of **3a**, which was fixed to the value corresponding to a minimum in R_G.

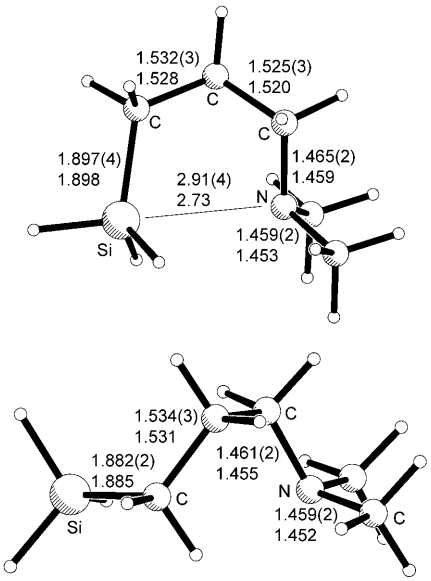

Figure 14. Molecular geometries of **3a** and **3b** showing selected GED (upper values, where the values in parentheses are σ) and MP2/TZVPP distances.

Topology of the electron density: We recently showed for $(F_3C)F_2SiONMe_2$[7] and $F_3SiONMe_2$[18] that, despite the presence of relatively short Si···N distances and acute angles at the oxygen atoms in the three-membered SiON rings, the electron-density topology analysed in terms of the quantum theory of atoms in molecules (QTAIM)[19] describes these as open-chain systems. This means that no bond paths (bp) or bond critical points (bcp) between silicon and nitrogen atoms can be found in the electron-density maps, although the electron-density distribution and its features are similar to those of related non-cyclic silane–amine adducts along the Si–N vectors. It is thus of interest whether the long Si···N interaction in the five-membered ring system of conformer **3a** would show the electron density topology of a normal silane–amine adduct. For this purpose the electron density was calculated from the wave function obtained at the MP2/TZVPP level of theory and analysed in terms of the QTAIM approach. Selected results are listed in Table 5 and the electron density and Laplacian maps are displayed in Figures 15 and 16.

The bond paths derived from the charge density recover the molecular graph drawn from classical chemical considerations, including the Si···N bonding interaction. Note that

Table 5. Parameters of the electron-density topology for selected bonds in **3a** in the calculated ground state, obtained at the MP2/TZVPP level of theory: Distances of the bond critical points (bcp) to the nuclear positions along the bond paths [Å], electron densities $\rho(r_{BCP})$ [e Å^{-3}], Laplacians $\nabla^2\rho(r_{BCP})$ [e Å^{-5}] and ellipticities ε at the bcp.

A–B	d(A–bcp)	d(B–bcp)	$\rho(r_{bcp})$	$\nabla^2\rho(r_{bcp})$	ε
Si···N	1.253	1.485	0.15	0.96	0.55
Si–H_{anti}	0.717	0.768	0.78	6.08	0.05
Si–H_{gauche}	0.713	0.758	0.80	6.43	0.01
Si–H_{gauche}	0.714	0.758	0.80	6.27	0.02
Si–C	0.722	1.177	0.78	5.67	0.04
N–C_{Me}	0.865	0.588	1.84	−17.7	0.04
N–C_{Me}	0.857	0.597	1.80	−16.1	0.08
N–C_{ring}	0.870	0.589	1.83	−17.3	0.04
C_N–C	0.770	0.749	1.72	−16.0	0.03
C_{Si}–C	0.760	0.768	1.65	−14.4	0.01

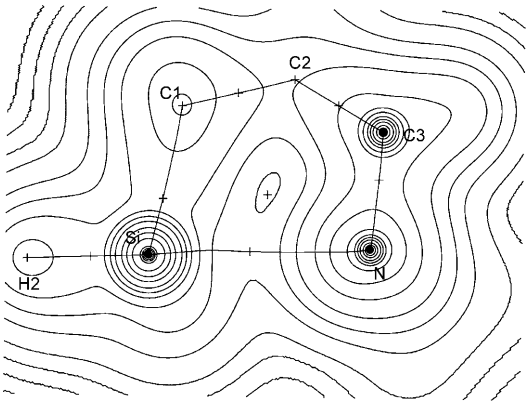

Figure 15. Calculated electron-density map for **3a** obtained at the MP2/TZVPP level of theory, showing bond-critical points as solid dots (lines printed at values of 0.002×10^n, 0.004×10^n and 0.008×10^n e Å^{-1}, with $n=$ 0, 1, 2, 3…).

© 2008 Wiley-VCH Verlag GmbH & Co. KGaA, Weinheim

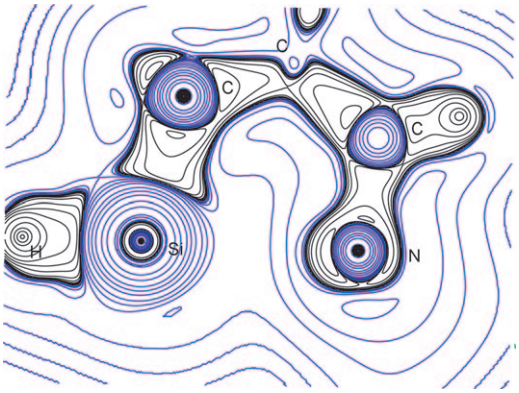

Figure 16. Calculated map of the Laplacian of the electron density for **3a** obtained at the MP2/TZVPP level (lines printed at values of $\pm 0.002 \times 10^n$, $\pm 0.004 \times 10^n$ and $\pm 0.008 \times 10^n$ e Å^{-1}, with $n = 0, 1, 2, 3, \ldots$). Positive values are printed as blue and negative values as black lines.)

the Si···N distance in the equilibrium geometry of the underlying calculations is shorter than experimentally determined by GED.

Most of the bonds show the typical values of the descriptors used to characterise their nature in bonding. The C–C and N–C bonds have all high electron densities and negative Laplacian values at their bcps, indicative of their covalent nature. In contrast the Si–H bonds and even the Si–C bond have values of less than half the density of the former and positive Laplacians. This is normally seen as an indication for closed-shell or ionic interactions.

In this respect the electron-density topology is similar to that of other hypervalent silicon compounds such as the hexacoordinate difluorobis[*N*-(dimethylamino)phenylacetimidato-*N*,*O*]silicon with an SiO_2F_2 core plus two nitrogen donor substituents, recently investigated by Stalke et al.[20] This compound has much shorter and stronger Si···N interactions than **3a**, and consequently we find a much smaller electron density at the bcp of the Si···N bonding interaction for **3a** of 0.15 e Å^{-3} compared with difluorobis[*N*-(dimethylamino)phenylacetimidato-*N*,*O*]silicon (0.50 e Å^{-3}). The description of the Si···N interaction in **3a** as a closed-shell interaction follows from the positive Laplacian value, but its magnitude is much less than those of the other bonds about the silicon atom and also less than in the compound investigated by Stalke et al. The relatively high ellipticity of 0.55 at the bcp is noteworthy, but care is suggested in not over-interpreting this value due to the low electron density at this bcp.

The Laplacian plot of **3a** (Figure 16) shows the local charge concentration at the nitrogen atom, which corresponds to the lone pair of electrons. It points towards the silicon atom, which is charge-depleted. Despite the very low electron density along the bond path in **3a**, it seems to be this alignment of charge accumulation and depletion in conjunction and the absence of another large electron density basin in close proximity which makes the Si···N bond path determinable in this case. In $(F_3C)F_2SiONMe_2$ the contribution of the oxygen electron density overlays the closed-shell Si···N interaction, and therefore a Si···N bond path cannot be found, although the electron density in this compound is more than three times higher at the minimum point on the Si–N vector.

Conclusions

The nature of the intramolecular Si··N interaction in *N*,*N*-dimethylaminopropyl silane (**3**) has been investigated by a number of experimental and theoretical techniques. The solid state consists of a single molecular conformation, arranged as a five-membered ring, which is a prerequisite for such an interaction. The Si···N distance of 2.719(2) Å and partial distortion of the coordination sphere around Si from a tetrahedral towards a trigonal-bipyramidal arrangement are indicative of a weak interaction. The ^{1}H and ^{29}Si NMR spectra of **3** exhibit similar chemical shifts and coupling constants for the SiH_3 group to those for the related compounds $H_3SiCH_2NMe_2$ (**1**) and $H_3Si(CH_2)_2NMe_2$ (**2**), for which the Si···N interaction ought to be very weak or absent. Variable-temperature ^{1}H and ^{29}Si NMR spectra exhibit some changes in the chemical shifts, but no significant change in the ^{1}H coupling constants, and hence a strong interaction in solution is ruled out.

Infrared spectra also provide information regarding this interaction by way of the Si–H stretching frequencies and intensities in the region 2000–2200 cm^{-1}. In cyclic conformer **3a**, approach of the nitrogen atom towards silicon weakens the Si–H bond *trans* to the nitrogen atom and results in splitting of the absorption band. This effect is most pronounced in the solid phase, but is also clearly observable in the liquid- and gas-phase spectra. The calculated relative intensities for cyclic conformer **3a** and seven open-chain conformers **3b–h** could be used to determine the abundance of **3a** in the gas phase to be 23.7(6) % by fitting the measured IR absorptions. This value was confirmed independently by GED (24(6) %), whilst the abundances predicted by theory vary from 12 to 44 % at the HF and MP2 levels, respectively. As **3a** is not the dominant conformer in the gas phase, the Si···N interaction must be relatively weak. However, given the large number of possible conformations, the presence of this conformer in significant proportions is indicative of a stabilising intramolecular interaction.

The Si···N distance obtained by GED of 2.91(4) Å lies between the values predicted by HF and MP2 theory of 3.14 and 2.73 Å, and is very close to an interpolated CCSD[T] value (see Figure 10). As was observed in similar cases, it is significantly longer than in the solid state.[11] The large discrepancy between the geometries calculated at HF and MP2 levels in this case is a consequence of the shallow deformation potential in **3a**, which causes high sensitivity of the Si···N distance to small effects like electronic correlation contributions treated differently at varying levels of theory. So the Si···N interaction is not purely electrostatic in character, but must also have contributions from dispersion inter-

 © 2008 Wiley-VCH Verlag GmbH & Co. KGaA, Weinheim

actions, which are unaccounted for in HF, overestimated by MP2[14] and more accurately described in CCSD[T].

Despite **3a** having a long and weak Si···N interaction, according to the quantum theory of atoms in molecules a bond path and bond critical point are found between silicon and nitrogen. This is in contrast to $(F_3C)F_2SiONMe_2$ and $F_3SiONMe_2$, which have three-membered rings and a much stronger Si···N interaction, but no detectable bond path and bond critical point.

This work has demonstrated that only the combination of many experimental and theoretical methods allows detailed insight into the complicated conformational behaviour of such a simple compound as $H_3Si(CH_2)_3NMe_2$ and a consistent description of a system determined by a weak intramolecular dative bond.

Experimental Section

General: All reactions were carried out under a dry and oxygen-free argon or nitrogen atmosphere by using standard Schlenk techniques. Solvents were purified by using standard methods and were distilled under inert-gas atmosphere prior to use. All compounds other than those mentioned below were commercially available. NMR measurements were carried out a Bruker Avance 400 and a Bruker Avance 200 spectrometer. Chemical shifts are reported in parts per million (ppm) with reference to the residual solvent signals for ^{1}H and ^{13}C NMR spectroscopy, to tetramethylsilane for ^{29}Si NMR spectroscopy and to trichlorofluoromethane for ^{19}F NMR spectroscopy. IR spectra were recorded on a Midac Prospect IR spectrometer. Liquid compounds were analysed as a film between two KBr plates.

General preparation procedure for aminoalkyl silanes: Lithium aluminium hydride was suspended in diethyl ether. At 0°C (*N*,*N*-dimethylaminoalkyl)trimethoxysilane was slowly added with stirring of the reaction mixture. The suspension was stirred overnight and allowed to warm to room temperature. The volatile compounds were separated from the solid by-products by condensation. The aminoalkyl silanes can be isolated by distillation and purified by fractional distillation.

(*N*,*N*-Dimethylaminoethyl)silane (2): The starting material (*N*,*N*-dimethylaminoethyl)trimethoxysilane was prepared by a literature procedure.[21] For the preparation of **2** the general procedure mentioned above was applied using lithium aluminium hydride (0.91 g, 24 mmol), diethyl ether (40 mL) and (*N*,*N*-dimethylaminoethyl)trimethoxysilane (3.86 g, 20 mmol). The product (1.70 g, 16.5 mmol, 83%) was isolated as a clear liquid upon distillation at 47°C and 500 mbar. ^{1}H NMR (400 MHz, $CDCl_3$, 25°C) δ = 0.85 (m, 2H; $SiCH_2$), 2.08 (s, 6H; NCH_3), 2.26 (t, ^3J(H,H) = 7.9 Hz, 2H; CH_2N), 3.37 (t, ^3J(H,H) = 3.8 Hz; SiH_3); ^{13}C NMR (100 MHz, $CDCl_3$, 25°C) δ = 5.1 (t, ^1J(C,H) = 122 Hz; SiC), 44.6 (q, ^1J(C,H) = 133 Hz; NCH_3), 56.4 (t, ^1J(C,H) = 133 Hz; NCH_2); ^{29}Si NMR (79 MHz, $CDCl_3$, 25°C) δ = −62 (q, ^1J(Si,H) = 195, ^3J(H,H) = 3.8 Hz; Si); IR (gas phase): $\tilde{\nu}$ = 619 (w), 703 (w), 760 (w), 860 (w), 937 (vs, SiH_3), 1052 (m), 1143 (s, NMe_2), 1362, 2151 (s, SiH), 2783 (m, CH), 2870 (m, CH), 2981 cm^{-1} (m, CH); MS (70 eV): *m*/*z* (%): 103 (8) [M^+], 72 (8) [M^+−SiH_3], 59 (26) [M^+−NMe_2], 58 (100) [$CH_2NMe_2^+$], 44 (12) [NMe_2^+], 31 (60) [SiH_3].

(*N*,*N*-Dimethylaminopropyl)silane (3): The general procedure mentioned above was applied using lithium aluminium hydride (0.91 g, 24 mmol), diethyl ether (40 mL) and (*N*,*N*-dimethylaminopropyl)trimethoxysilane (4.15 g, 20 mmol). The product was purified by fractional condensation on a vacuum line. The pure product was isolated at −40°C, while in the cold trap held at −78°C a mixture of product and diethyl ether was isolated, which could by purified by repeated condensation (1.68 g, 14.4 mmol, 72%). M.p. −102°C; ^{1}H NMR (400 MHz, $CDCl_3$, 25°C) δ = 0.69 (m, 2H; $SiCH_2$), 1.15 (m, 2H; CCH_2C) 2.12 (s, 6H; NCH_3), 2.20 (t, ^3J(H,H) = 7.2 Hz, 2H; NCH_2), 3.44 (t, ^3J(H,H) = 3.9 Hz; SiH_3); ^{13}C NMR (100 MHz, $CDCl_3$, 25°C) δ = 3.9 (t, ^1J(C,H) = 121 Hz; SiC), 24.1 (t, ^1J(C,H) = 127 Hz; CCH_2C), 45.2 (q, ^1J(C,H) = 133 Hz; NCH_3),61.7 (t, ^1J(C,H) = 131 Hz; NCH_2); ^{29}Si NMR (79 MHz, $CDCl_3$, 25°C) δ = −60 (q, ^1J(Si,H) = 193 Hz; Si); IR (gas phase): $\tilde{\nu}$ = 604 (w), 687 (w), 802 (w), 938 (vs, SiH_3), 1043 (w), 1144 (w), 1267 (w), 1466 (m), 2107 (s, SiH), 2160 (vs, SiH), 2780 (m, CH), 2824 (m, CH), 2945 cm^{-1} (m, CH); MS (70 eV): *m*/*z* (%): 117 (7) [M^+], 86 (7) [M^+−SiH_3], 59 (25) [M^+−CH_2NMe_2], 58 (100) [$CH_2NMe_2^+$], 44 (10) [NMe_2^+], 43 (14) [$C_3H_7^+$], 31 (67) [SiH_3].

Crystal-structure determination: A single crystal of $H_3SiCH_2CH_2CH_2NMe_2$ was grown by slowly cooling the melt after establishing a solid–liquid equilibrium of the sample in a sealed glass capillary. All but one of the crystals (an optically selected, very small seed crystal) were then melted by locally warming the sample. Data were collected on a Nonius Kappa CCD diffractometer. Graphite-monochromated $Mo_{K\alpha}$ radiation was used (λ = 0.71073 Å). Crystal data: space group *I*4*m*, *a* = 14.992(1), *c* = 8.976(1) Å, *V* = 2017.3(2) Å^3, *T* = 108(2) K, 20909 scattering intensities measured, 1548 of which were unique (R_{int} = 0.0546). The structure was solved by direct methods and refined with the full-matrix least-squares procedure (SHELXTL)[22] against F^2. The hydrogen atoms at Si1 were refined isotropically, and the other hydrogen atoms at calculated positions by using a riding model. The unit cell contains two voids, each with a volume of 219 Å^3, with indefinable electron density, which was removed by using the SQUEEZE program.[23] To exclude the presence of impurities like disordered solvent molecules in these voids, the crystallisation experiments were repeated four times with independent samples. The sealed capillaries were checked before and after the diffraction experiments by NMR spectroscopy for purity and no change was observed. CCDC 689072 contains the supplementary crystallographic data for this paper. These data can be obtained free of charge from The Cambridge Crystallographic Data Centre via www.ccdc.cam.ac.uk/data_request/cif.

Computational details: All calculations (but DF-LCCSD[TF]/TZVPP single points of **3a**) were performed with the TURBOMOLE program package (version 5.7),[24] and geometries were optimised by using redundant internal coordinates[25] and employing either the TURBOMOLE dscf routine[26] (RHF level of theory), the RI-MP2[27–30] level of theory (using the TURBOMOLE RI-CC2 routine[28–30] and frozen core orbitals) or density functional theory[31,32] using the BP86 local density functional,[33–38] the RI-method[39] in connection with the m3 quadrature[34,38] (denoted in the article as RI-DFT) or the PBE0 gradient density functional[43–45] in connection with the m4 quadrature[37,42] (denoted in the article as DFT). For partially optimised (MP2) geometries of **3a** (at Si···N distances of 2.728 (MP2 equilibrium geometry), 2.8, 2.9 and 3.0 Å, single-point energies at the DF-LCCSD[T]/TZVPP (fully iterative triples treatment) were calculated with MOLPRO (2006.1).[15]

Basis sets of either SV(P)[38] or TZVPP quality[48] in connection with the corresponding auxiliary basis sets for RI-DFT[36,37] and for RI-MP2[29,47] were used for all elements. All converged structures were verified as minima by frequency analyses. For the RI-DFT level of theory this was done by using the aoforce routine, while for all other levels of theory, the NumForce routine was used.[48]The following abbreviations for the level of theory are used in this work: RI-DFT = RI-DFT/SV(P) for RI-DFT-(BP86)/SV(P)/grid m3; DFT = DFT/TZVPP for DFT(PBE0)/TZVPP/grid m4; HF = HF/TZVPP, MP2 = MP2/TZVPP = RI-MP2(fc)/TZVPP; CCSD[T] = RI-MP2(fc)/TZVPP//DF-LCCSD[T]/TZVPP.

GED experimental and computational details: Electron scattering intensities for **3** were recorded at room temperature on reusable Fuji imaging plates by using a Balzers KD-G 2[49] Gas-Eldigraph at the University of Bielefeld (formerly operated in Tübingen by H. Oberhammer[50]), equipped with a new electron source (STAIB Instruments), operating at about 50 kV and with a beam current of about 200 nA. During data acquisition the background pressure rose from 1.3×10^{-6} to 2.5×10^{-5} mbar, and the optimal exposure time was 45–60 s. Exposed imaging plates were scanned with a commercially available Fuji FLA 3000 scanner to yield digital 16-bit grey-scale image data. The image data were reduced to total intensities by using T. G. Strand's program PIMAG[51] (version 040827) in connection with a sector curve, which is based on experimen-

 © 2008 Wiley-VCH Verlag GmbH & Co. KGaA, Weinheim

tal xenon diffraction data and tabulated scattering factors of xenon. Further data reduction (yielding molecular-intensity curves), the molecular structure refinement, and the electron wavelength determination (from benzene data) were performed with version 2.4 of the ed@ed program.[52] The scattering factors employed were those of Ross et al.[53] Further details about the Bielefeld GED apparatus and methods will be published elsewhere.[54] Table S1 (Supporting Information) gives the data analysis parameters for each data set: R factors (R_D and R_G), scale factors, correlation parameter values, data ranges, weighting points, nozzle-to-plate distances and electron wavelengths. Amplitudes of vibration u and distance corrections for curvilinear perpendicular motion k_{h1} were calculated by using the program SHRINK,[55] making use of frequency calculations at the MP2/6-31G** level of theory,[56,57] performed with the Gaussian 03 software package.[58]

GED model: All bonded distances were used in the models, with a separate average distance for each atom-pair type. Where the differences between bonded distances of the same type were calculated to be greater than 0.002 Å, these differences were also included as parameters. The only exceptions were the C–H distances, which, given the low scattering cross-section for hydrogen, were assumed to be identical. Local symmetry was assumed for all hydrogen atom positions, although that of the SiH_3 group in **3a** was lowered to C_s, whereas C_{3v} symmetry was applied to the other conformers. The main difference in the models of the different conformers was in the description of the Si-C-C-C-N chain. For **3a** this was described in terms of a five-membered ring, so that the Si···N distance could be refined directly. In the other three conformers the heavy-atom chain was described in z-matrix form. The geometry around the nitrogen atom was calculated to be similar for all four conformers, and thus a single average C-N-C angle was assumed, although within each conformer one of these angles was allowed to differ from the others. A full list of independent parameters and detailed descriptions can be found in Table S2 in the Supporting Information.

GED refinement: The geometries and relative abundances of the four conformers calculated at the MP2/TZVPP level served as a starting point for the GED refinement. Prior to refining any of the geometric parameters, the fraction of each conformer was varied then fixed at the value corresponding to a minimum in the R factor (R_G). This was done in the order **3a**, **3b** then **3c** (the fraction of **3d** was dependent on the others) until self-consistency was achieved. The molecular geometries were then refined by the SARACEN method[14] with restraints calculated at the MP2/TZVPP level of theory. The only parameters refined completely unrestrained were the average C–H and Si–C bond lengths and Si···N distance in **3a**. The average C–C, C–N and Si–H distances were refined with restraints on the differences [C–C minus C–N] and [C–N minus Si–H]. The remaining parameters describing the geometry of the five-membered ring in **3a** were mostly refined without restraints being applied directly, as were the average Si-C-C angle, and the combined average of the C-C-C and C-C-N angles in **3b–d**. However, the difference between the Si-C-C angles in **3a** and **b** were restrained, as were those for the C-C-C and C-C-N angles. Little information was contained in the GED data for the remaining parameters. This is evident from Table S1 (Supporting Information), in which the values of these parameters are close to those of the restraints and e.s.d. similar to the uncertainties are placed on the restraints. Fifteen amplitudes of vibration were refined, with restraint uncertainties of 5% of the calculated values and with those corresponding to distances under a single peak in the radial-distribution curve tied together. Following preliminary refinement of the geometry and amplitudes of vibration, further scans of the R factor as functions of the conformer ratios were performed. These conformer ratios were then fixed to those corresponding to the minima in Figure 13, and at this point the final set of refined parameter values was obtained.

Acknowledgement

The authors are grateful to the Graduate School of Chemistry at the Westfälische Wilhelms-Universität in Münster for financial support (to M.H.) and to the Deutsche Forschungsgemeinschaft (SPP 1178). We thank Prof. Dr. Pekka Pyykkö and Dr. Dage Sundholm (Helsinki) for generous provision of computational resources and Dr. Andreas Mix (Bielefeld) and Dr. Alexander Hepp (Münster) for NMR measurements.

[1] a) A. Bauer, T. Kammel, B. Pachaly, O. Schäfer, W. Schindler, V. Stanjek, J. Weis in *Organosilicon Chemistry V* (Eds.: N. Auner, J. Weis), Wiley-VCH, Weinheim, **2003**, p. 527; b) One Step Ahead—Organofunctional Silanes from Wacker, Wacker Co., available from http://www.wacker.com/internet/webcache/de_DE/_Downloads/GENIOSIL_Brosch_en.pdf; c) S. Giessler, B. Standke, *Farbe Lack* **2005**, *4*, 134–139; d) A Guide to Silane Solutions from Dow Corning, Dow Corning Co., available from http://www.dowcorning.com/content/publishedlit/SILANE-GUIDE.pdf.

[2] a) J. E. Noll, B. F. Daubert, J. L. Speier, *J. Am. Chem. Soc.* **1951**, *73*, 3871. b) L. H. Sommer, J. Rockett, *J. Am. Chem. Soc.* **1951**, *73*, 5130.

[3] R. G. Kostyanovskii, A. K. Prokof'ev, *Dokl. Akad. Nauk SSSR* **1965**, *164*, 1054.

[4] a) J. Boyer, C. Breliere, R. J. P. Corriu, A. Kpoton, M. Poirier, G. Royo, *J. Organomet. Chem.* **1986**, *311*, C39–C43; b) R. J. P. Corriu, C. Guerin, B. J. L. Henner, W. W. C. Wong Chi Man, *Organometallics* **1988**, *7*, 237; c) S. E. Johnson, J. A. Deiters, R. O. Day, R. R. Holmes, *J. Am. Chem. Soc.* **1989**, *111*, 3250.

[5] a) C. Chuit, R. J. P. Corriu, C. Reye, J. C. Young, *Chem. Rev.* **1993**, *93*, 1371; b) M. A. Brook, *Silicon in Organic, Organometallic and Polymer Chemistry*, Wiley-VCH, Weinheim, **2000**; c) K.-y. Akiba, *Hypervalent Compounds*, Wiley-VCH, Weinheim, **1998**.

[6] N. W. Mitzel, K. Vojinović, T. Foerster, H. E. Robertson, K. B. Borisenko, D. W. H. Rankin, *Chem. Eur. J.* **2005**, *11*, 5114.

[7] N. W. Mitzel, K. Vojinović, R. Fröhlich, T. Foerster, H. E. Robertson, K. B. Borisenko, D. W. H. Rankin, *J. Am. Chem. Soc.* **2005**, *127*, 13705.

[8] K. Vojinović, L. J. McLachlan, S. L. Hinchley, D. W. H. Rankin, N. W. Mitzel, *Chem. Eur. J.* **2004**, *10*, 3033.

[9] N. W. Mitzel, U. Losehand, B. Bauer, *Inorg. Chem.* **2000**, *39*, 1998.

[10] N. W. Mitzel, U. Losehand, *J. Am. Chem. Soc.* **1998**, *120*, 7320.

[11] K. R. Leopold, M. Canagaratna, J. A. Philips, *Acc. Chem. Res.* **1997**, *30*, 57.

[12] N. W. Mitzel, C. Kiener, D. W. H. Rankin, *Organometallics* **1999**, *18*, 3437.

[13] J.-P. Kintzinger, H. Marsmann, *Oxygen-17 and Silicon-29*, Springer, Berlin, **1981**.

[14] S. Grimme, *Chem. Eur. J.* **2004**, *10*, 3423.

[15] MOLPRO, version 2006.1, a package of ab initio programs, H.-J. Werner, P. J. Knowles, R. Lindh, F. R. Manby, M. Schütz, and others see http://www.molpro.net.

[16] a) A. J. Blake, P. T. Brain, H. McNab, J. Miller, C. A. Morrison, S. Parsons, D. W. H. Rankin, H. E. Robertson, B. A. Smart, *J. Phys. Chem.* **1996**, *100*, 12280. b) N. W. Mitzel, D. W. H. Rankin, *Dalton Trans.* **2003**, 3650.

[17] W. C. Hamilton, *Statistics in Physical Science*, Ronald, New York, **1964**.

[18] N. W. Mitzel, U. Losehand, A. Wu, D. Cremer, D. W. H. Rankin, *J. Am. Chem. Soc.* **2000**, *122*, 4471

[19] a) R. F. W. Bader, *Atoms in Molecules—A Quantum Theory*, Oxford University Press, Oxford, **1990**. b) *The Quantum Theory of Atoms in Molecules: From Solid State to DNA and Drug Design* (Eds.: C. M. Matta, R. J. Boyd), Wiley-VCH, Weinheim, **2007**.

[20] N. Kocher, J. Henn, B. Gostevskii, D. Kost, I. Kalikhman, B. Engels, D. Stalke, *J. Am. Chem. Soc.* **2004**, *126*, 5563.

[21] a) B. Pfrommer, R. Tacke, *Eur. J. Inorg. Chem.* **1998**, 415–418; b) R. Tacke, B. Pfrommer, M. Pülm, R. Bertermann, *Eur. J. Inorg. Chem.* **1999**, 807.

[22] SHELXTL 6.10, Bruker-AXS X-Ray Instrumentation Inc., Madison, WI, **2000**.

[23] R. Ahlrichs, M. Bär, M. Häser, H. Horn C. Kölmel, *Chem. Phys. Lett.* **1989**, *162*, 165.

 © 2008 Wiley-VCH Verlag GmbH & Co. KGaA, Weinheim

[24] R. Ahlrichs, M. Bär, M. Häser, H. Horn C. Kölmel, *Chem. Phys. Lett.* **1989**, *162*, 165.
[25] M. von Arnim, R. Ahlrichs, *J. Chem. Phys.* **1999**, *111*, 9183.
[26] M. Häser, R. Ahlrichs, *J. Comput. Chem.* **1989**, *10*, 104.
[27] R. Ahlrichs, *Phys. Chem. Chem. Phys.* **2004**, *6*, 5119.
[28] F. Weigend, M. Häser, *Theor. Chem. Acc.* **1997**, *97*, 331.
[29] F. Weigend, M. Häser, H. Patzelt, R. Ahlrichs, *Chem. Phys. Lett.* **1998**, *294*, 143.
[30] F. Haase, R. Ahlrichs, *J. Comput. Chem.* **1993**, *14*, 907.
[31] A. Köhn, C. Hättig, *J. Chem. Phys.* **2003**, *119*, 5021.
[32] M. Sierka, A. Hogekamp, R. Ahlrichs, *J. Chem. Phys.* **2003**, *118*, 9136.
[33] C. Hättig, *J. Chem. Phys.* **2003**, *118*, 7751.
[34] P. A. M. Dirac, *Proc. R. Soc. London Ser. A* **1929**, *123*, 714.
[35] J. C. Slater, *Phys. Rev.* **1951**, *81*, 385.
[36] K. Eichkorn, O. Treutler, H. Öhm, M. Häser, R. Ahlrichs, *Chem. Phys. Lett.* **1995**, *242*, 652.
[37] K. Eichkorn, F. Weigend, O. Treutler, R. Ahlrichs, *Theor. Chem. Acc.* **1997**, *97*, 119.
[38] A. Schäfer, H. Horn, R. Ahlrichs, *J. Chem. Phys.* **1992**, *97*, 2571.
[39] S. H. Vosko, L. Wilk, M. Nusair, *Can. J. Phys.* **1980**, *58*, 1200.
[40] A. D. Becke, *Phys. Rev. A* **1988**, *38*, 3098.
[41] J. P. Perdew, *Phys. Rev. B* **1986**, *36*, 8822.
[42] O. Treutler, R. Ahlrichs, *J. Chem. Phys.* **1995**, *102*, 346.
[43] J. P. Perdew, Y. Wang, *Phys. Rev. B* **1992**, *45*, 13244.
[44] J. P. Perdew, K. Burke, M. Ernzerhof, *Phys. Rev. Lett.* **1996**, *77*, 3865.
[45] J. P. Perdew, M. Ernzerhof, K. Burke, *Chem. Phys.* **1996**, *105*, 9982.
[46] A. Schäfer, C. Huber, R. Ahlrichs, *J. Chem. Phys.* **1994**, *100*, 5829.
[47] R. Ahlrichs, K. May, *Phys. Chem. Chem. Phys.* **2000**, *2*, 943.
[48] P. Deglmann, K. May, F. Furche, R. Ahlrichs, *Chem. Phys. Lett.* **2004**, *384*, 103.
[49] W. Zeil, J. Haase, L. Wegmann, *Z. Instr.* **1966**, *74*, 84.
[50] H. Oberhammer in *Molecular Structure by Diffraction Methods, Vol. 4* (Eds.: G. A. Sim, L. E. Sutton), The Chemical Society, London, **1976**, p. 24.
[51] S. Gundersen, S. Samdal, T. G. Strand, H. V. Volden, *J. Mol. Struct.* **2007**, *832*, 164.
[52] S. L. Hinchley, H. E. Robertson, K. B. Borisenko, A. R. Turner, B. F. Johnston, D. W. H. Rankin, M. Ahmadian, J. N. Jones, A. H. Cowley, *Dalton Trans.* **2004**, 2469.
[53] A. W. Ross, M. Fink, R. Hilderbrandt in *International Tables for Crystallography, Vol. C* (Ed.: A. J. C. Wilson), Kluwer, Dordrecht, **1992**, p. 245.
[54] R. J. F. Berger, N. W. Mitzel, unpublished results.
[55] V. A. Sipachev, *J. Mol. Struct.* **1985**, *121*, 143.
[56] C. Møller, M. S. Plesset, *Phys. Rev.* **1934**, *46*, 618.
[57] P. C. Hariharen, J. A. Pople, *Theor. Chim. Acta* **1973**, *28*, 213.
[58] Gaussian 03 (Revision C.02), M. J. Frisch, G. W. Trucks, H. B. Schlegel, G. E. Scuseria, M. A. Robb, J. R. Cheeseman, J. A. Montgomery, Jr., T. Vreven, K. N. Kudin, J. C. Burant, J. M. Millam, S. S. Iyengar, J. Tomasi, V. Barone, B. Mennucci, M. Cossi, G. Scalmani, N. Rega, G. A. Petersson, H. Nakatsuji, M. Hada, M. Ehara, K. Toyota, R. Fukuda, J. Hasegawa, M. Ishida, T. Nakajima, Y. Honda, O. Kitao, H. Nakai, M. Klene, X. Li, J. E. Knox, H. P. Hratchian, J. B. Cross, V. Bakken, C. Adamo, J. Jaramillo, R. Gomperts, R. E. Stratmann, O. Yazyev, A. J. Austin, R. Cammi, C. Pomelli, J. W. Ochterski, P. Y. Ayala, K. Morokuma, G. A. Voth, P. Salvador, J. J. Dannenberg, V. G. Zakrzewski, S. Dapprich, A. D. Daniels, M. C. Strain, O. Farkas, D. K. Malick, A. D. Rabuck, K. Raghavachari, J. B. Foresman, J. V. Ortiz, Q. Cui, A. G. Baboul, S. Clifford, J. Cioslowski, B. B. Stefanov, G. Liu, A. Liashenko, P. Piskorz, I. Komaromi, R. L. Martin, D. J. Fox, T. Keith, M. A. Al-Laham, C. Y. Peng, A. Nanayakkara, M. Challacombe, P. M. W. Gill, B. Johnson, W. Chen, M. W. Wong, C. Gonzalez, J. A. Pople, Gaussian, Inc., Wallingford, CT, **2004**.

Received: June 20, 2008
Published online: October 30, 2008

 © 2008 Wiley-VCH Verlag GmbH & Co. KGaA, Weinheim